frontiers in Energy Research

ORIGINAL RESEARCH
published: 06 November 2020
doi: 10.3389/fenrg.2020.596062

Commonalities of Atomic Layer Deposition of Oxide Coatings on Activated Carbons for 3.5 V Electric Double Layer Supercapacitors

Daniel Q. Tan, Guanghui Song, Dayakar Gandla and Fuming Zhang*

Technion Israel Institute of Technology Institute and Guangdong Technion Israel Institute of Technology, Shantou, China

High voltage electric double layer capacitors with reliable cycling performance are in high demand for energy storage applications. In this research, studies of the process-structure-property relations of commercial activated carbon electrode modified with atomic layer deposition (ALD) have been performed in terms of coating of various oxide compounds. These investigations have yielded similar enhancements of cycling performance at high voltages (3.5 V) enabled by the ALD coating of oxides on activated carbon surfaces. The commonalities are the phenomenal increase in capacitance retention of coin cell supercapacitors after 1,000 charge/discharge cycles regardless of the electric nature of ALD deposited oxides. Minor differences in coating morphologies and uniformities were observed between the aluminum oxide, titanium oxide, and manganese-cobalt oxide. ALD coating of these oxides of about 20-growth cycle (1–2 nm in thickness) was found to effectively result in reliable cycling performance, lower impedance, and significantly low leakage current. The authors proposed a modified Gouy-Chapman-Stern model to explain the remarkable increase in operating voltage and cycling performance by the increased Stern layer thickness due to the ALD oxide coating. These results demonstrate that the ALD oxide coating has excellent potential for activated carbons for high operating voltage and energy density supercapacitor.

Keywords: atomic layer deposition, activated carbon, metal oxide, high voltage, supercapacitors

OPEN ACCESS

Edited by:
Arul Manuel Stephan,
Central Electrochemical Research Institute (CSIR), India

Reviewed by:
Emilia Morallon,
University of Alicante, Spain
Jose Rajan,
Universiti Malaysia Pahang, Malaysia
Ramiro Ruiz Rosas,
University of Malaga, Spain

****Correspondence:***
Daniel Q. Tan
daniel.tan@gtiit.edu.cn

Specialty section:
This article was submitted to Electrochemical Energy Conversion and Storage, a section of the journal Frontiers in Energy Research

Received: *18 August 2020*
Accepted: *06 October 2020*
Published: *06 November 2020*

Citation:
Tan DQ, Song G, Gandla D and Zhang F (2020) Commonalities of Atomic Layer Deposition of Oxide Coatings on Activated Carbons for 3.5 V Electric Double Layer Supercapacitors. Front. Energy Res. 8:596062. doi: 10.3389/fenrg.2020.596062

INTRODUCTION

An electric double layer capacitor (EDLC) is constructed when both positive and negative electrodes are made of carbon-based materials, such as activated carbon (AC), and electrolytes. The conventional ACs have dominated the commercial electrochemical supercapacitor market for their high surface area, high electric conductivity, temperature stability, excellent cycling stability, and low-cost manufacturing (Kotz and Carlen., 2000; Wang et al., 2009; Noh et al., 2013). However, the specific energy of carbon supercapacitors is limited to ~5–20 Wh kg^{-1}, which is still much inferior to lithium-ion batteries (LIBs). AC electrodes commonly suffer from high leakage current, especially under a high operating voltage of 2.5–3.0 V, which results in self-discharge and low efficiency charging/discharging cycles with a significant amount of energy waste(Balducci et al., 2007; Liu et al., 2019). This is because the decomposition of the electrolyte at the electrode surface contains functional groups with electrocatalytic and irreversible electrochemical reactions at the interface(Oda et al., 2006; Beguin et al., 2014; Xiao et al., 2015; Miller et al., 2018). Reduction in the

density of oxygen-containing functional groups and hydrophilic groups can increase the stability of AC electrodes in nonaqueous electrolytes (Kim et al., 2014; Dong et al., 2018). More electron-rich functional groups such as N introduced into the delocalized pi-system of the carbon network also increases electrical conductivity and capacitance (Hulicova-Jurcakova et al., 2009; Shen et al., 2014; Chi et al., 2016; Yang et al., 2017). Recently, Simon and Gogotsi pointed out in Nature Materials that efforts should be directed toward the modification of the porous carbon/electrolyte interface by preparing passive layers or designing specific properties for more opportunities to enlarge the operation voltage range of EDLC device (Simon and Gogotsi., 2020). Therefore, it is the right approach to engineer the surface chemistry of ACs without using expensive ionic liquids to achieve enhanced voltage stability and electrochemical characteristics in an electric double layer capacitor.

Vijayan and co-workers have developed thin metal oxide coated porous carbon derived from a highly abundant non-edible bio resource to achieve a high-performance supercapacitor electrode (Vijayan et al., 2019). Wu's group developed the uniform and dense porous carbon film of 3D-crosslinked nanoscale network structure through microwave plasma-assisted chemical vapor deposition (MPCVD) (Wu et al., 2017). Arico's group presented a grand strategy to tune the morphology and the properties of sputtered porous Nb_2O_5 thin films deposited on Si-based substrates via the magnetron sputtering technique (Arico et al., 2019). Compaired with the solution-based sol-gel coating, molecular layer deposition (MLD), magnetron sputtering and hydrothermal reaction, the ALD offers skinny conformal coating that penetrates into tortuous electrodes. By exposing the substrate to different precursors alternately, one atomic layer of the deposited species is grown after one cycle of sequential exposure to each precursor. The different surface chemical reactions serve as effective protection layers thus leading to better cycling ability. The unique role in controlling the film thickness at the Ångstrom scale and facilitating coverage of high aspect-ratio substrates bring a great hope for the applications of ALD in energy storage. **Table 1** compares the performance of various techniques benchmarking the achievements in making films on porous carbon.

Atomic layer deposition (ALD) has proven the effectiveness of conformal coating of ultrathin layers at three-dimensional structures of energy materials for the increased cyclic performance at higher voltages owing to the surface passivation of carbons or Li-rich battery electrodes (Chen et al., 2010; Liu et al., 2012; Jung et al., 2013; Gandla and Tan., 2019). Lin et al. (2019) modified the solid electrolyte interphase of carbon materials for Na-ion batteries by ALD coating of 1 nm Al_2O_3 nanoclusters on 3D porous graphene monolith scaffold. The ultrathin oxide coating effectively blocked the electrolyte's direct contact with the active sites on carbon, suppressing the decomposition of the electrolyte during the cyclic operation. Yair's group developed fluoride coating of a few atomic layers on Li-rich powder and electrodes resulting in an enhanced cycle life without compromising the cathode performance and a higher cutoff voltage (4.5 V) (Shapira et al., 2018). Su et al. (2019) ALD Ta_2O_5 layer effectively prevented the dissolution of the active materials and enhanced the electrodes' phase stability by inhibiting the interfacial interactions between the NMC532 and the electrolyte. Li et al. (2019) utilized a CuO based composite electrode with ALD passivation of ternary FeO_x and TiO_2 to obtain an ultrahigh Li-ion storage capacity of 1,585 mA h g^{-1} and excellent cycle performance by TiO_2 shell's accommodation of the volume variation of Fe_3O_4. These superior results in battery cells further triggered the exploration of the ALD technique to improve AC electrodes for high voltage reliable supercapacitor performance.

Seeing the advantages of ALD, Tan and Zhao (2014) disclosed an innovative approach in their patent application, applying an ultrathin aluminum oxide coating on the commercial AC electrodes using the ALD technique, which leads to a >3.5 V operating window for the EDLCs. The Al_2O_3-encapsulation added a thin layer of dielectric material on the AC surface, which may increase the thickness of the Stern layer and thus decreases the electrical leakage. Hong et al. (2015) also reported 3 V-stable AC electrodes by encapsulating AC with ultrathin ALD Al_2O_3 layer, and high energy and power densities of 46 Wh kg^{-1} and 86 kW kg^{-1}, respectively. The authors are very curious if there is a common positive effect for the ALD coating of various materials on improving cycling performance of EDLC cells? What is the fundamental role of ALD coating on the carbons? What type of coating morphology is sufficient to enable an EDLC to operate at >3.5 V?

According to the Gouy–Chapman-Stern model, the total voltage drop across the electric double layer is the sum of voltage at the diffuse layer (V_D) and Stern layer (V_{St}). V_D is proportional to the Debye length and the total charge per unit surface (Q) in the diffuse region, and inversely proportional to the dielectric permittivity of the electrolyte (ε_r) according to the Gouy–Chapman surface charge–voltage relationship for small surface charge (Kondrat et al., 2012). In comparison with aqueous electrolytes, organic electrolytes are intrinsically capable of working under higher voltages for larger ionic size (d_{St}) and lower dielectric permittivity (65 for propylene carbonate, 36 for acetonitrile, 80 for water). The intrinsically higher working voltage of organic electrolytes cannot be realized when the Stern layer thickness is small. To enable higher working voltages (>3 V) for the organic electrolytes, one needs to increase Stern layer thickness by using larger ions such as ionic electrolytes or introducing an additional dielectric layer on the carbon surface for organic electrolytes. As a result of the carbon surface encapsulation, the thicker effective Stern layer and the Debye diffuse layer ($d_{Stern} + \lambda_D$) can withstand higher operating voltages regardless of the surface functional groups or defects of carbons. However, the additional dielectric layer should be kept sufficiently thin to avoid the decrease of nanopore surface area and the ion transport path.

The authors designed a set of experiments utilizing four different kinds of dielectric materials (low dielectric permittivity insulating aluminum oxide, medium dielectric permittivity mixed zinc-aluminum oxide, high dielectric permittivity titanium oxides (semiconducting/conducting reduced oxygen in thin films), and conducting magnetic manganese cobalt oxide). Using a commercial AC electrode as an ALD substrate to deposit these

TABLE 1 | The performance comparison between different film coating methods on carbons.

Materials	Methods	Application	Performance	References
Activated carbons	ALD	Supercapacitor	88% of capacitance retained after 5,000 cycles at 70°C at 3 V	Hong et al., 2015
Carbon nanotubes	ALD	Supercapacitor	92% of capacitance Retention after 5,000 cycles at 5 A g^{-1}	Boukhalfa et al., 2012
Porous carbon	MPCVD	Supercapacitor	95% of capacitance retention after 10,000 cycles	Wu et al., 2017
Micro/Mesoporous carbon	CVD	Supercapacitor	Good cyclability, down to 90% of the initial value (100 F g^{-1}) after 10,000 cycles	Smolin et al., 2017
Si-based substrates	Magnetron sputtering	Lithium-ion battery	Surface capacity close to 60 μAh cm^{-2} at 1 mV s^{-1}	Arico et al., 2019
Mesoporous carbon	Sol-gel	Supercapacitor	Specific capacitance of 242 F g^{-1} and stable over 10,000 cycles	Qian et al., 2016
Graphene	MLD	Supercapacitor	High specific capacitance of 290.2 F g^{-1} at 1 A g^{-1}	Chen et al., 2016

oxides, the authors report commonalties in the electrochemical performances of all encapsulated AC electrodes that showed improved operating voltage over 3.5 V and charge-discharge retention in this work. It is encouraging to observe the suppression of undesired Faradaic effect and life expectancy decrease due to encapsulating insulating double layers.

EXPERIMENTAL AND SAMPLES

Materials

AC powders were YP-50F from Kuraray, and the AC electrodes were fabricated on Al foils by a Chinese supercapacitor manufacturer. It has a typical morphology and electrical performance as published elsewhere (Ma et al., 2013).

Synthesis of Atomic Layer Deposition Oxide Coated Activated Carbons

ALD coating was carried out using a Benchtop GESTar XT-D ALD system as commercially provided by Arradiance, Inc. Aluminum oxide (Al_2O_3), mixed zinc-aluminum oxide (25% ZnO-Al_2O_3), titanium oxides (TiO_{2-x}), and manganese cobalt oxide compound ($MnCo_{2-x}O_4$) are targeted at various depositing conditions using the following precursors: Trimethyl Aluminum (TMA), Diethyl Zinc (DEZ), Titanium (IV) Isopropoxide (TIP), Manganese (II) Acetylacetonate [$Mn(acac)_2$], Cobalt (III) Acetylacetonate [$Co(acac)_3$], and high-performance liquid chromatography grade H_2O (HPLC, Sigma-Aldrich). The mixed precursors of TMA:DEZ = 4:1 and $Mn(acac)_2$:$Co(acac)_3$ = 1:2 coworking with precursor H_2O for the depositions of 25% ZnO-Al_2O_3 and $MnCo_2O_4$, respectively. The critical properties of these oxides are listed in **Table 2** (Gronera et al., 2002; Ju et al., 2013; Lanje et al., 2013; Barroso-Bogeat et al., 2014; Meena et al., 2014). Typical chemical reactions in this work follow the equations below (Zhao and Wang., 2013):

$Al(CH_3)_3 + H_2O \rightarrow Al_2O_3 + CH_4$; $Zn(CH_2\ CH_3)_2 + H_2O \rightarrow ZnO + CH_3\ CH_3$; TIP + $H_2O \rightarrow TiO_2 + CH_3\ CH_2\ CH_3$; $Mn\ (acac)_2 + H_2O \rightarrow MnO_2 + CH_3COOH$;

$Co(acac)_3 + H_2O \rightarrow Co_2O_3 + CH_3COOH$.

The typical growth rate for the chemistry is 0.5–1.5 Å per cycle for dielectric oxide materials. Using Al_2O_3 as an example, the reaction sequence within each deposition cycle was: 1) exposure of the substrate to TMA, 2) purge to remove the nonreacted precursors and the byproducts, 3) exposure of the substrate to H_2O, 4) purge to remove the nonreacted precursors and the byproducts.

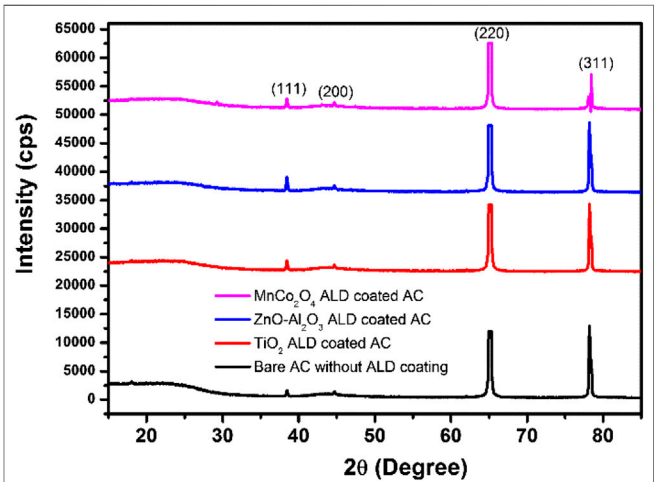

FIGURE 1 | XRD patterns for AC electrodes with and without ALD coating of $MnCo_2O_4$, ZnO-Al_2O_3, and TiO_2. The four major peaks are from the Al substrate.

The activated carbon electrodes (not powders) were first vacuum dried overnight at 100°C to dehumidify and purify. The substrates were fixed onto a silicon wafer with Kapton tape and placed into the ALD chamber. Each ALD process was conducted at 150°C chamber temperature with a constant argon gas flow rate of 10 sccm. During each deposition cycle, a computer-controlled pneumatic exhaust valve between the flow chamber and the exhaust pump was closed first. Two different reactant precursors were pulsed alternately into the chamber with the pulsing time of 0.2 s (s). A purging with a duration of 6 s was required between two subsequent pulses. The substrate electrodes were transferred into clean zip-lock storage bags or used for electrochemical performance tests immediately after deposition.

Characterization

The crystallographic structures of bare AC and ALD oxides-coated AC electrodes were examined using a Smartlab nine X-ray diffractometer at a scan rate of 6°/min using 150 mA current, 40 kV voltage and copper target. The surface morphology and

TABLE 2 | Electric and magnetic properties of materials of interest for ALD.

Materials	Dielectric permittivity (10 kHz)	Magnetic permeability	Electrical conductivity (S/m)	Remark
Al_2O_3	3.5–9 (thickness dependent)	1	10^{-13} (20°C)	ALD thin film, insulating (Groner et al., 2002)
25% ZnO-Al_2O_3	<17	1	$<10^{-4}$ (600°C)	Nanoparticles, insulating (Lanje et al., 2013)
TiO_{2-x}	<103	1	>10 (sensitive to O/Ti ratio, 20°C)	Amorphous thin film, conducting (Ju et al., 2013)
$MnCo_{2-x}O_4$	2,500 (100 kHz)	>1	100 (400°C)	Thin film and bulk, conducting and magnetic (Meena et al., 2014; Szymczewska et al., 2017)
Carbon	N/A	1	194	Bulk, conducting (Barroso-Bogeat et al., 2014)

particle size were observed using a ZEISS Sigma-500 field emission scanning electron microscopy. The elemental distribution and mapping were obtained using Energy Dispersive Spectroscopy (EDS, BRUKE XFlash-6130, Germany). Transmission electron microscopy (TEM) images were captured on a JEM2100 instrument at an acceleration voltage of 200 kV, to understand the features of oxide encapsulation. Specific surface areas were determined by BET tests using Quantachrome Autosorb-iQ2-MP (USA) and nitrogen isotherms with degassing at 250°C for 3 h for each 36 mg sample. X-ray photoelectron spectroscopy was taken using Thermo Scientific ESCALAB 250Xi (USA) and monochromatic Al target.

Electrochemical Measurements

The supercapacitive performance of the AC and ALD coated AC electrodes was evaluated by making a symmetrical supercapacitor device through CR2032 coin using the Gamry electrochemical workstation (Interface 1010E, USA). Coin cells were assembled in a glovebox by maintaining water and O_2 levels <0.01 ppm. Before this, the electrodes were first vacuum dried at 50°C for 12 h. 1 M $TEABF_4$/acetonitrile was used as electrolyte. A 35-μm thick cellulose NKK TF4035 (Nippon Kodoshi, Japan), having 75% porosity was used as a separator. Aluminum foil with 20 μm in thickness was used as a current collector. According to information from the Chinese supercapacitor manufacturer, the working electrodes were prepared by homogeneously mixing of YP-50F AC powder (~85%), super P carbon black (~10%), and polyvinylidene difluoride (~5%) in N-methyl-2-pyrrolidinone solution, and then a vortex mixer was used for 15–30 to achieve a homogeneously mixed carbon slurry. The carbon slurry was then spread onto a sheet of current collector (aluminum foil) with a doctor blade technique to produce a homogenous film. Afterward, this coated film was vacuum dried at 90°C for 12 h, and the final thickness of the coated AC was ~100 μm. Finally, it was pressed to a dense sheet at 10 MPa to obtain working electrodes. The electrodes were cut into circular disks with a diameter of 1.13 cm^2 using an MTI disk cutting machine (MSK-T10), the loaded active mass on each working electrode was found to be ~2.2–2.4 mg cm^{-2}. Galvanostatic charge-discharge (GCD) measurements were carried out between 5 and 100 mA cm^{-2}. EIS data were recorded with 5 mV amplitude potential within 10 kHz–0.01 Hz frequency range.

The specific capacitance (C, F g^{-1}), energy density (E, Wh kg^{-1}), and Coulombic efficiency (η) values of the coin cell supercapacitor were calculated using GCD curves from the following equations (Yan et al., 2020).

$$C = \frac{I\Delta t}{m\Delta V} \quad (1)$$

$$E = \frac{C \times \Delta V^2}{2 \times 3.6} \quad (2)$$

$$\eta = \Delta t_d/\Delta t_c \times 100\% \quad (3)$$

where I represents the discharge current (A), Δt is the discharge time (s), m is the total mass (g) of active material loaded on both the electrodes, ΔV denotes the applied potential window (V), and $\Delta t_d/\Delta t_c$ is the ratio of discharge time to charge time.

RESULTS AND DISCUSSIONS

Microstructural Analysis for Atomic Layer Deposition Coated Activated Carbon Electrodes

Al_2O_3 coating by ALD is the most mature process using TMA precursors with a deposition temperature ranging from 60 to 200°C. Numerous work has been reported to successfully form the conformal coating of the Al_2O_3 layer on various substrates. However, nanometer-thick alumina are not readily present in the crystalline phase, so XRD and other imaging techniques were used to detect their coating status. XRD pattern of AC particles coated with 20 ALD growth cycles of aluminum oxide, zinc oxide, and titanium oxide is displayed in **Figure 1**. The patterns of the three different materials following the ALD processing conditions for the respective precursors, as described in the experimental section, do not show the signals for the crystalline oxide phases except those peaks belonging to the aluminum substrate. The deposition of the $MnCo_2O_4$ compound using thermal-mode ALD technique has not been reported before. This work uses the pre-mixed precursors of Mn $(acac)_2$ and $Co(acac)_3$ to attempt its formation. Their diffraction peaks are not detectable either, indicating the amorphous nature of the compounds or nonstoichiometric composition $MnCo_{2-x}O_4$. The morphology analysis and elemental imaging were conducted using FESEM and EDS, respectively, to verify the coating effect.

Figure 2A shows the in-plan view of SE scattering images of a typical region of the AC electrodes. The ALD coated oxides are highlighted in **Figure 2B** by the elemental mapping images. The cross-section image contrast in **Figures 2C,D** presents a rich message of 25% ZnO-Al_2O_3 coating and intensity contour of secondary electron scattering. The particle edges and surfaces are

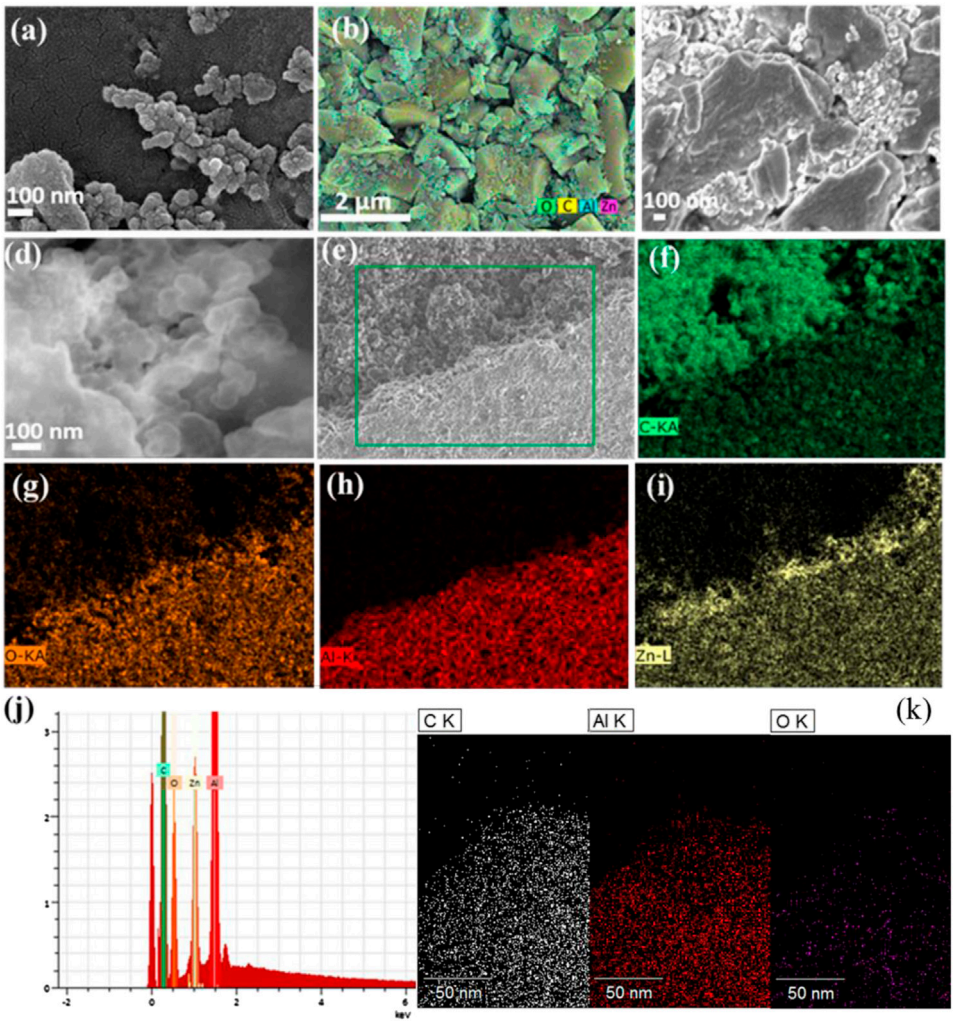

FIGURE 2 | SEM images of AC electrodes without coating **(A)** and coated with the ZnO-Al_2O_3 mixture **(B–D)**. EDS elemental distribution of various elements in ZnO-Al_2O_3 coating showing their presence at the bottom of AC electrodes **(E–I)** and its elemental mapping **(J)**. EDS elemental mapping of ALD Al_2O_3 coated AC electrodes taken in TEM.

lighter, and the center area of the particles is darker in image contrast, indicating the heavier elements on the surface. The activated carbon electrodes are considered to possess rough tortuous surfaces with a depth of about 100 microns. The extent to which the deposited oxide layer conforms to the tortuous surface of the conductive active layer and the uniformity of coating coverage on the surface depends on the precursor material's ability to penetrate into the high-aspect-ratio features of the surface. Since ALD introduces reactants into the deposition chamber as gasses in pulses at preselected times, with each pulse resulting in a reaction of the gasses with the substrate surface, the oxide coating is successfully realized at both surfaces of the AC electrode and the vicinity of the Aluminum foil substrate.

Figure 2E shows the SEM image at the bottom region of the AC electrode proving the excellent step coverage on high aspect ratio structures. **Figures 2F–I** are the elemental mapping of the ALD coating at the bottom of the electrode. Similar mapping distribution is observed on the top and bottom locations suggesting the in-depth presence of Zn oxide and Al oxide. The EDS analysis for both locations also confirms the penetration of 25% ZnO-Al_2O_3 down to the substrate despite a slightly higher Al/Zn ratio in the surface region (**Figures 2G–J**). The ALD Al_2O_3 coated AC images are similar to those of ZnO-Al_2O_3 coated (not shown), as shown by the elemental mapping in **Figure 2K**.

Similar SEM images were observed for AC electrodes coated with TiO_{2-x} and $MnCo_{2-x}O_4$, where both nonstoichiometric compounds are well known to be formed in thin-film growth (Ju et al., 2013; Lanje et al., 2013). **Figure 3A** shows the typical area of a TiO_{2-x} coated AC electrode comprising AC particles and binders. **Figure 3B** exhibits its elemental mapping showing the presence of Ti element. Likewise, $MnCo_{2-x}O_4$ compound was also deposited into AC electrodes for different coating conditions, as shown in **Figures 3C,D**. The phase formation is relatively difficult even after attempted 2,000 cycles deposited at 175°C.

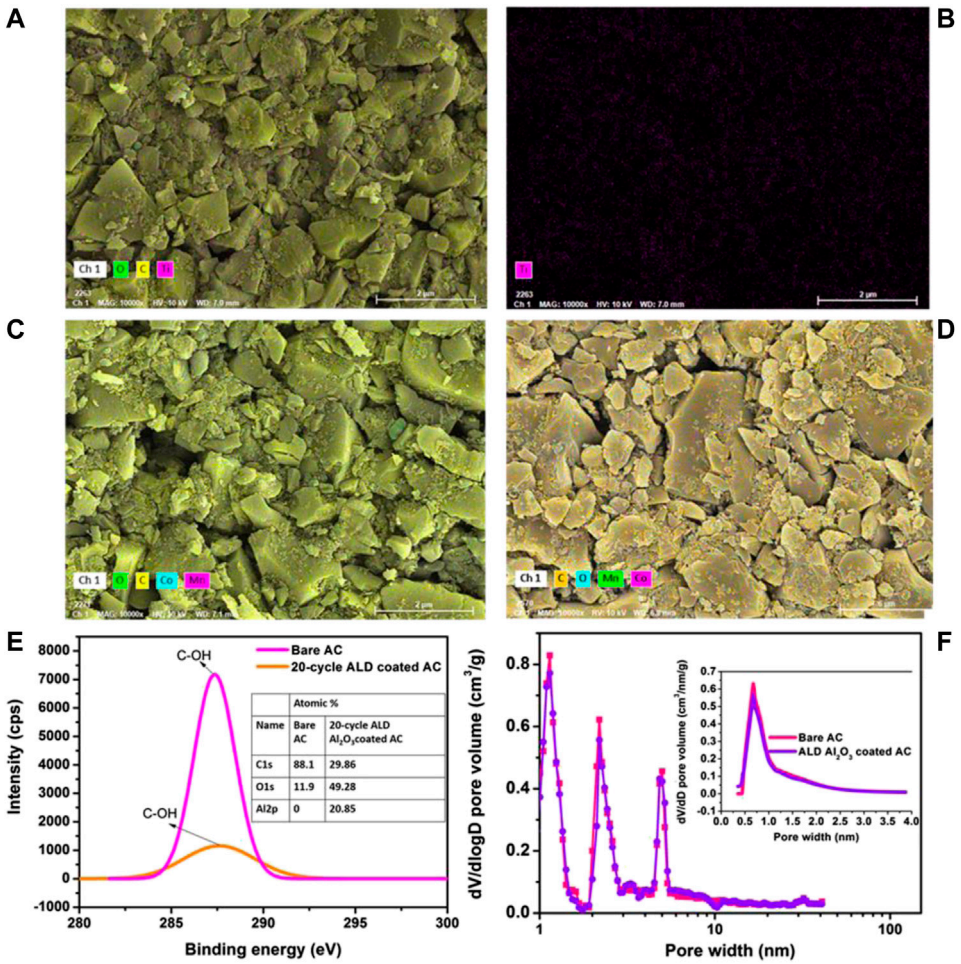

FIGURE 3 | SEM images for AC electrodes coated with TiO_{2-x} **(A,B)** and $MnCo_{2-x}O_4$ **(C,D)**. **(E)** XPS C 1 s spectrum (C-OH) of AC before and after ALD modification, the inset shows atomic% of various elements. **(F)** Pore size distribution of bare AC and ALD modified AC using DFT method and the inset shows their pore distribution by HK method.

X-ray photoelectron spectroscopic (XPS) analysis was carried out to know the effect of ALD modification on the surface functional groups of AC by considering one of the oxide-coated AC, i.e., Al_2O_3 coated AC. The deconvoluted C 1s XPS spectrum (**Figure 3E**) shows that the peak intensity of hydroxyl (C-OH) groups of AC at 287 eV decreased significantly after ALD modification, and an increase in overall oxygen atomic% from 11.9 to 49.2% was observed. This implies that the 2 nm oxide layer replaced many of the oxygen functional groups present on the surface of AC. In order to understand if metal oxide coating blocks micropores, we have carried out the pore structure analysis (or pore size distribution) of ALD-modified AC in comparison with bare AC using DFT (density functional theory) and HK (Horvath-Kawazoe) methods from N_2 adsorption-desorption isotherms (at 77.4 K). This pore analysis is represented in **Figure 3F**. The BET specific surface area, pore volume of the bare AC and ALD Al_2O_3 modified AC were found to be 2,142 $m^2\,g^{-1}$, 0.39 $cm^3\,g^{-1}$ and 2,005 $m^2\,g^{-1}$, 0.38 $cm^3\,g^{-1}$, respectively. The 6.4% less in pore volume implies that the ALD modification does not decrease surface area and pore volume significantly, similar to other reports (Hong et al., 2015). The DFT shows that peak intensities of micro- and mesopores of bare AC slightly decreased after ALD coating but peak position and pore width are almost similar. The mean pore width of bare and ALD modified AC from the DFT method were found to be 0.56 and 0.54 nm, respectively. The HK method available for micropore ($d \leq 2$ nm) smaller than coating thickness did not detect any change in pore diameter after ALD coating (inset of **Figure 3F**). As a result, the ALD coating does not block neither mesopore nor micropore channels of AC.

To explore the details of ALD oxide coatings, TEM images were taken to reveal its thin layer morphology on the surface of carbon. **Figure 4** presents the images of AC particles and the surrounding oxide encapsulation. The coatings are all observed, however they are non-conformal when viewing various locations. Al_2O_3 layer of about 2 nm in thickness can be seen clearly (**Figures 4A,B**). ZnO–Al_2O_3 coating is also observed in the EDS spectra reveal the elements of C (0.3 keV), O (0.5 keV), Al (1.5 keV), Ti (4.5 keV), and Cu (at 8.0 keV), respectively (**Figures 4C,D**). The Cu peaks come from the copper grid

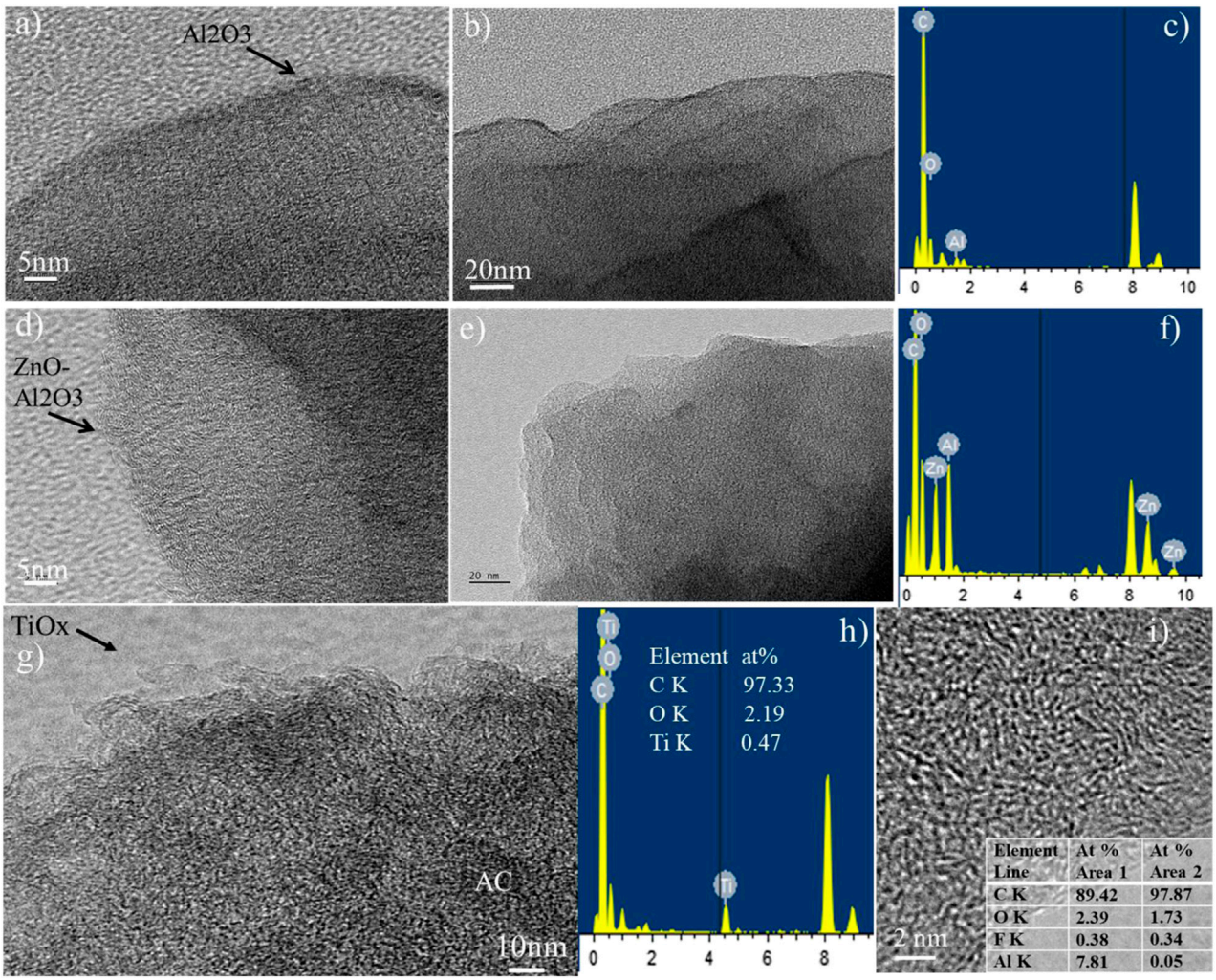

FIGURE 4 | TEM images and EDS of AC electrodes coated with 20-cycle ALD Al_2O_3 **(A–C)**, 20-cycle ALD ZnO-Al_2O_3 **(D–F)**, and TiO_{2-x} **(G,H)**, TEM image and EDS elemental concentration **(I)**.

where the TEM sample is placed. It is noted that the atomic percentages of Ti, Al, and O are 0.47%, 0.38%, and 2.19–3.38%, respectively, depending on the location of inspection. This confirms the formation of TiO_{2-x} and Al_2O_3 coating on the surface of the AC particle. However, the additional O element from EDS analysis indicates the presence of oxygen-containing functional groups on the surface of AC electrodes. The quantitative EDS analysis for all ALD coated AC samples is shown in **Table 3**. All the information suggests adding a layer of oxides on top of AC particles regardless of being conformal or not.

TABLE 3 | Elemental compositions in various AC electrode samples.

ALD oxide	C, at%	O, at%	Al, at%	Zn at%	Ti, at%	Mn, at %	Co, at %
Al_2O_3	89.42	2.39	7.81	—	—	—	—
ZnO-Al_2O_3	78.90	14.30	4.69	2.11	—	—	—
TiO_{2-x}	91.26	6.70	—	—	2.04	—	—
$MnCo_{2-x}O_4$	92.45	6.80	—	—	—	0.11	0.65

Galvanostatic Charge-Discharge and Cycling Life Performance

As shown in **Figure 5A**, the shape of the charge-discharge curve of AC is well maintained without significant distortion after the 20-cycle ALD coating of various oxide materials. This is also confirmed by CV analysis (**Figure 5G**), as bare AC and ALD oxide coated ACs have shown similar quasi-rectangular shaped CV curves without a significant difference in the CV current. The specific capacitance of the 20-cycle ALD coated AC supercapacitor measured from GCD curves at 5 mA cm^{-2} is found to be 58–63 F g^{-1}, which is almost similar to that of bare AC (57 F g^{-1}). This implies that the porous structure was well maintained without the pore blocking issue during the thin

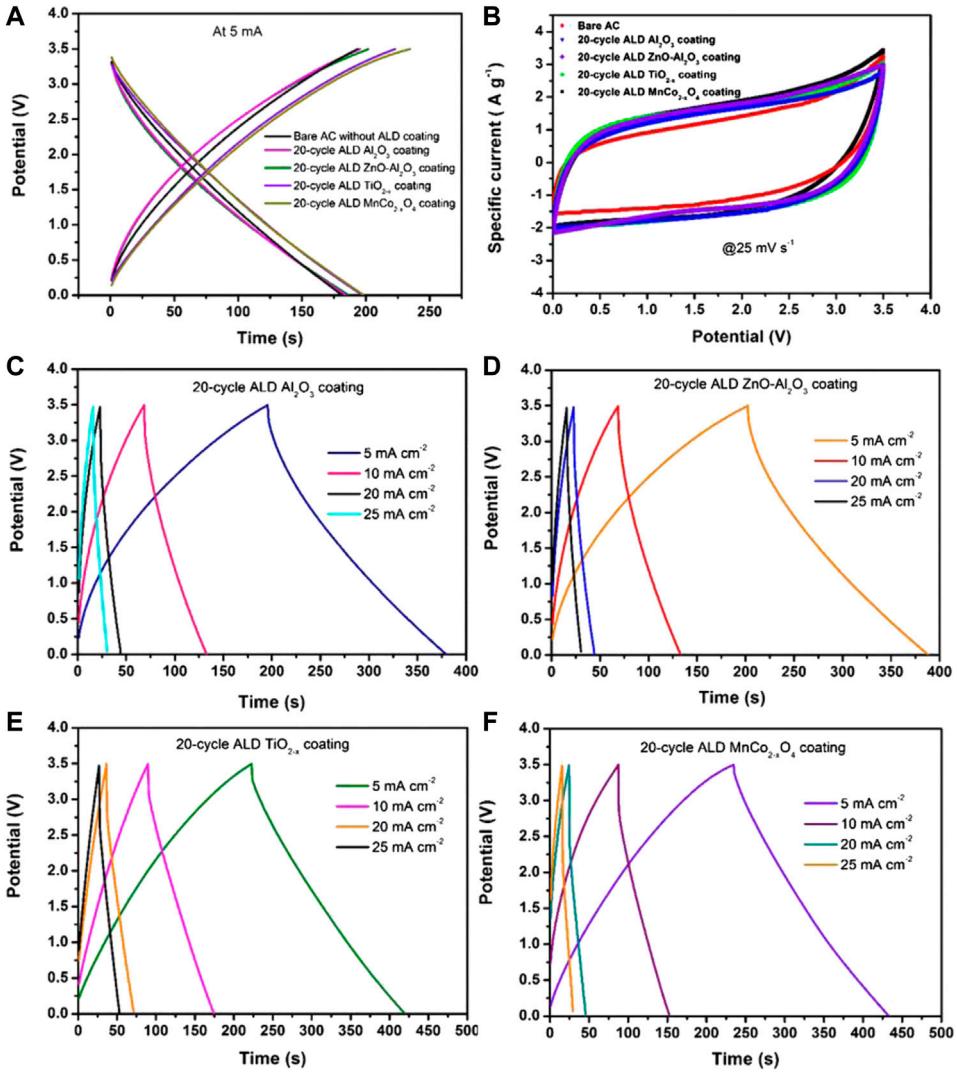

FIGURE 5 | (A) Galvanostatic charge-discharge curves of bare AC and various 20-cycle ALD oxide coated ACs at a current density of 5 mA cm^{-2}. **(B)** CV curves of bare AC and various ALD oxide coated ACs at a scan rate of 25 mV s^{-1}. **(C–F)** Galvanostatic charge-discharge curves of 20-cycle ALD coated Al_2O_3, ZnO-Al_2O_3, TiO_{2-x}, and $MnCo_{2-x}O_4$, respectively at various current densities from 5 to 25 mA cm^{-2}.

ALD coating. The various 20-cycle ALD oxide coated ACs have exhibited nearly symmetrical triangular shaped galvanostatic charge-discharge curves at different current densities (**Figures 5B–E**), which implies their excellent electrochemical reversibility and good capacitive behavior.

The ohmic drops (IR) of the ALD coated ACs were found to be 0.2–0.25 V at 2 mA cm^{-2}, and these values were increased with the increase in current densities to a maximum of 1–1.2 V at 25 mA cm^{-2}. These high ohmic drops are related to lower conductivity and large solvated ion size of TEA^+ (~1.3 nm) in the $TEABF_4$/ACN electrolyte system. Also, the hydrophilic nature and the high porosity of cellulose separator were reported to be another reason which provides rich interaction with the electrolyte solvent. Such interaction may lead to swelling of the separator and a decline of cellulose mechanical strength after immersion in the electrolyte, which induces poor contact between an electrode and a separator. Besides, ACN has a higher solvent reorganization energy compared to PC, which could cause additional ionic resistance in the case of the cellulose-solvent system (Safatri et al., 2020).

Coulombic efficiency (η) values measured for bare AC and ALD coated ACs are represented in **Table 4**. At low current densities (such as 5 and 10 mA cm^{-2}), it is in the range of 86%–97%. In contrast, at high current densities (such as 10 and 25 mA cm^{-2}), the values increase to the range of 98%–100% except for $MnCo_{2-x}O_4$ coated AC. The lower Coulombic efficiency at low current density should be attributed to the higher ratio of the parasitic side-chain reactions between the electrode and impurities present in the electrolyte (Chen et al., 2016). Interestingly, when the cycle life study is conducted at a further higher current of 100 mA cm^{-2}, all the electrodes including $MnCo_{2-x}O_4$ coated AC have exhibited a

TABLE 4 | Coulombic efficiencies of bare AC and ALD oxide coated ACs at different current densities.

Current density (mA cm^{-2})	Coulombic efficiencies (%)				
	ALD ZnO-Al_2O_3 coated AC	ALD ZnO-Al_2O_3 coated AC	ALD TiO_{2-x} coated AC	ALD $MnCo_{2-x}O_4$ coated AC	Bare AC
5	95	93.1	90.1	86.8	93.7
10	95.7	97.4	95.8	88.2	96
20	99.2	98.5	99.3	91	98.1
25	99.9	100.1	99.8	96	99.2

high Coulombic efficiency between 99% and 100%, which is represented in **Figures 6A–E** (including cycle life conducted till 5,000 cycles).

A supercapacitor suffers from the electrolyte decomposition during electrochemical cycling, especially at the high voltages and elevated temperatures due to undesirable parasitic side-chain reactions between electrolyte and abundant surface-active functional sites of electrode material, maintenance of cyclic life performance is the essential characteristic that needs to be ensured in new device development. Electrochemical cycling performance tests dedicated to this characteristic are carried out for bare AC, and ALD coated AC coin cell supercapacitors at 3.5 V and at a current density of 100 mA cm^{-2} (**Figure 6A**). The reference EDLC cell performance dramatically decreases after 1,000 charge/discharge cycles, as shown by its decreasing current carrying capability. On the contrary, there is a phenomenal increase in the retention performance of the AC electrode coated with a thin layer of insulating Al_2O_3, ZnO-Al_2O_3, conducting TiO_{2-x} (permittivity of 103), and conducting magnetic $MnCo_{2-x}O_4$ becomes better than that of the reference samples without ALD coating. It evidently demonstrates that commonalities exist in the ALD coating of oxides to improve capacitance retention and working voltage of AC-based EDLCs. ALD coating of 20 cycles can stabilize the capacitance retention at the optimum level (97%), which effectively prevents the electrolyte's reaction with the AC electrode during the electrochemical cycling. It is calculated that the 2 nm Al_2O_3 ALD coating delivers a final energy density of 57.3 Wh kg^{-1} after 1,000 electrochemical cycles at a voltage of 3.5 V. During cycling process, the symmetrical triangular shape of GCD curves of bare AC and ALD coated ACs is well maintained with a high Coulombic efficiency of 99%–100%. The representative curves of the first five (1–5th) and last five GCD cycles (996–1000th) are shown in **Figures 6C–G**. The loss of capacitance is evidenced in the case of bare AC as the charge-discharge time is reduced significantly at the end of cycle life. In contrast, the ALD oxide coated ACs have exhibited similarities in the charge-discharge duration. The IR drop has not increased with the increase in the cycle number, but a slight decrease in the IR drop is noticed.

Moreover, there are commonalities in the 20-cycle ALD coating effect of various oxides for the improvement of capacitance retention of AC for 1,000 cycles. Therefore, we have further carried out cycle life test till 5,000 GCD cycles by selecting one of the oxide-coated ACs, i.e., 20-cycle ALD Al_2O_3 coated AC by comparing with the bare AC (**Figure 6B**). Bare AC showed a less capacitance retention of 57%. In contrast, the Al_2O_3 coated AC showed a high retention of 81.2% along with a high Coulombic efficiency between 99% and 100%. The shape of the charge-discharge curves is almost similar during cycling process without any significant distortion and similar charge-discharge duration is observed, the representative curves after 10, 100, and 1,000 cycles are shown in **Figures 6B–E**. The IR drop does not increase with the increase in the cycle number, while a slight decrease in the IR drop is noticed.

A constant voltage holding test or float test is performed to further study the stability of ALD modified AC supercapacitor by considering one of the 20-cycle ALD oxide (Al_2O_3) coated ACs. The test was performed by galvanostatically cycling three times between 0 and 2.5 V in order to evaluate cell capacitance. After the cycling step, the cells were charged up to 3.25 or 3.5 V followed by holding the cell voltage for 5 h. The cell was then cycled again and the procedure was repeated until an overall holding period of 100 h was reached (Weingarth et al., 2013). The results of the holding test were differing significantly when the test was performed at two different voltages i.e., 3.25 and 3.5 V. At 3.25 V, an approximately 20% of capacitance loss was observed after holding the cells for 100 h. However, at 3.5 V, the capacitance loss was found to be ~50%. Moreover, the results of the stability test performed at 3.5 V by cycling test and holding test were also different. This is because the capacitor is exposed continuously to the maximum voltage during the holding tests, while the capacitor is exposed to a derated voltage during cycling tests.

Reduced Impedance in Activated Carbon Cells

Despite the previous advantage in cycling performance, oxide coating should neither block the micropores nor slow down the ionic transport rate. So, keeping the dielectric layer at minimal thickness is preferable for low impedance and short time constant. The ALD deposited oxides of all types in this work also turned out to be helpful. **Figure 7** depicts an oxide effect by the Nyquist plot of impedance/frequency performance of an uncoated reference supercapacitor and a supercapacitor, including a dielectric coating of about 2 nm. No increase in impedance has resulted from all types of oxide coating after cycling life tests. Instead, the impedances of AC cells with insulating Al_2O_3 and ZnO-Al_2O_3 layers are substantially reduced by ~30%, respectively compared with cells having uncoated AC (**Figures 7A,B**). The reduced resistance implies better contact between the electrolyte and surface of the electrode after the charge-discharge cycling test at 3.5 V.

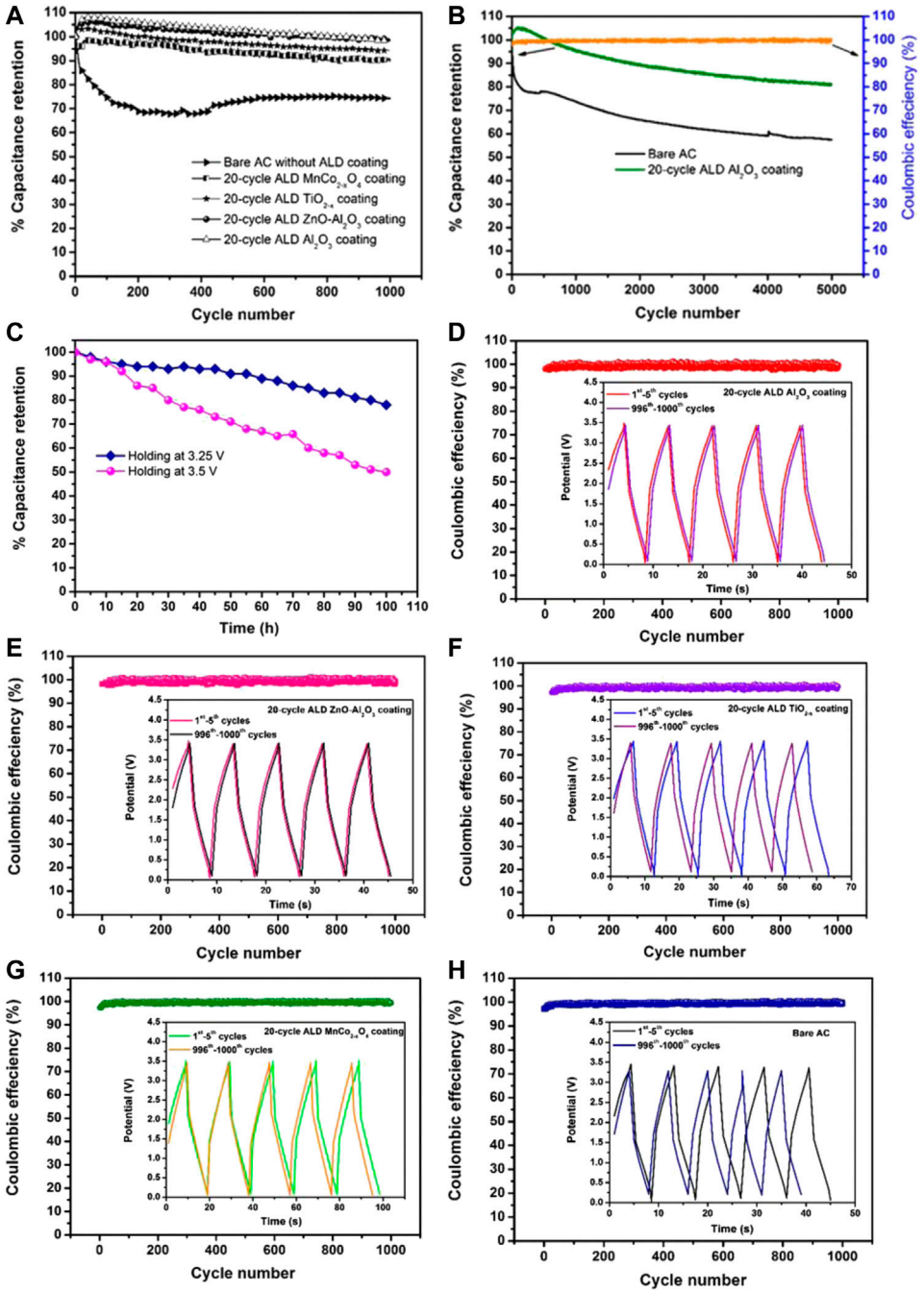

FIGURE 6 | (A) Capacitance retention of the bare AC and various ALD oxide coated AC electrodes carried out at 3.5 V and at a current density of 100 mA cm^{-2} till 1,000 cycles. **(B)** Capacitance retention of the bare AC and 20-cycle ALD Al_2O_3 coated AC electrodes for 5,000 GCD cycles. **(C)** Constant voltage holding test of 20-cycle ALD Al_2O_3 coated AC electrodes at 3.25 and 3.5 V **(D–H)** Coulombic efficiencies along with the representative shapes of GCD curves for 1–5th and 996–1000th cycles of 20-cycle ALD coated Al_2O_3, ZnO-Al_2O_3, TiO_{2-x}, $MnCo_{2-x}O_4$, and bare AC, respectively.

On the other hand, both TiO_{2-x} and $MnCo_{2-x}O_4$ coating do not reduce the impedance but increase the Nyquist plot slope a little, indicating the reduced electrical leakage due to the electrical conducting nature of the coating (**Figures 7C,D**). The minimal change with the $MnCo_{2-x}O_4$ coating may be due to the nonstoichiometric formation of the spinel phase in the current ALD processing. In any of these cases, the insertion of a thin dielectric layer between the AC particle surface and electrolyte has not shown an adverse effect on the ionic transport and time constant of power discharge of an EDLC cell.

The equivalent circuit model used to analyze the impedance data is shown as inset of **Figure 7A**. The charge-transfer

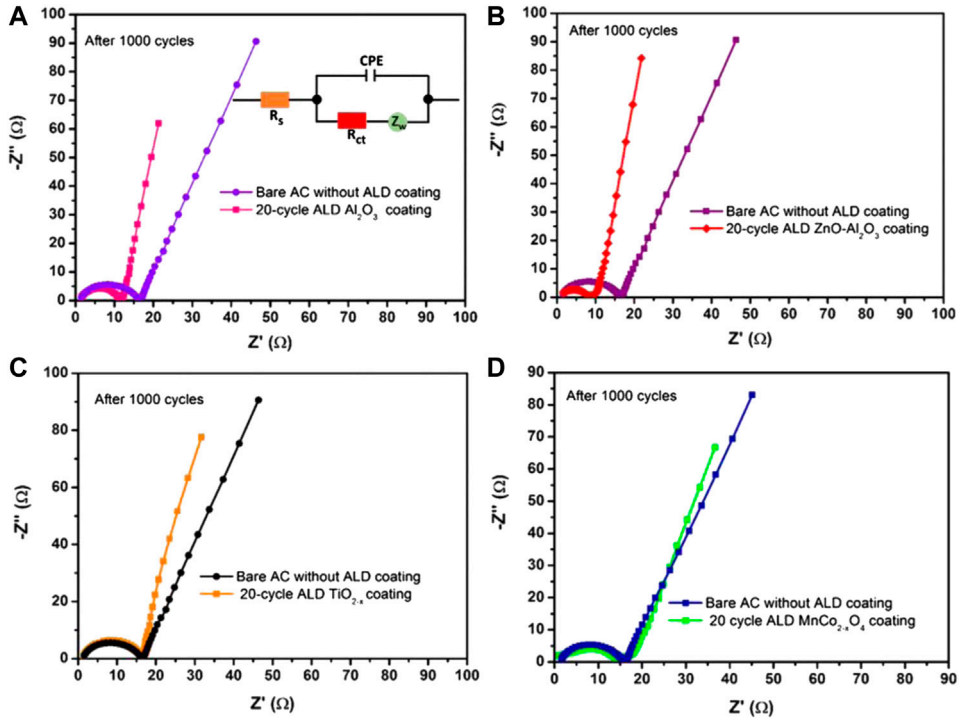

FIGURE 7 | Impedance behavior of AC-based cells with various coating materials after cycling tests. **(A)** Al_2O_3 coating; **(B)** ZnO-Al_2O_3 mixed coating; **(C)** TiO_{2-x} coating; **(D)** $MnCo_{2-x}O_4$ coating. The inset of **(A)** is the equivalent circuit model used to analyze impedance data of Nyquist plot.

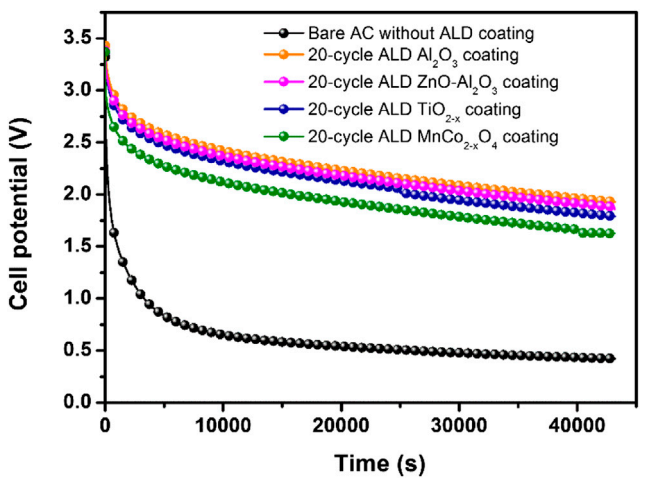

FIGURE 8 | Self-discharge profile of bare AC electrodes without ALD coating and with various ALD oxide coating of 20-cycle.

resistance (R_{ct}) values of the 20-cycle Al_2O_3, ZnO-Al_2O_3, TiO_{2-x}, and $MnCo_{2-x}O_4$ coated AC were found to be 10.26, 7.87, 15.1, and 13.82 Ω, respectively. Equivalent series resistance (R_s) values were 1.57, 1.5, 1.368, and 0.99 Ω respectively. This decrease in the R_s values from 20-cycle Al_2O_3 coated AC to $MnCo_{2-x}O_4$ coated AC is correlated with their increasing order of electrical conductivities mentioned in **Table 2**.

Self-Discharge Analysis

Leakage current is one of the most significant technical issues of present supercapacitors. To find any reduction in leakage current after ALD coating on the AC substrate, we have investigated the self-discharge profiles of bare AC and ALD coated ACs after charging them. The open-circuit potentials of the samples in **Figure 8** were measured for 12 h after charging for 1 h at the constant voltage of 3.5 V. The bare AC was maintained just 14% of its initial potential, whereas the ACs coated with 20-cycle Al_2O_3, ZnO-Al_2O_3, TiO_{2-x}, and $MnCo_{2-x}O_4$ maintained 54%, 57%, 60%, and 61% of their initial potentials, respectively. This considerable improvement once again proves the effectiveness and the commonalties of ALD oxide coating on stabilizing AC electrode performance.

Proposed Model for High Voltage Stability

The various results of four types of coating oxides demonstrate the less dependence on the electric nature of oxide materials. Both insulating and conducting oxides are favorable for the capacitance retention for higher working voltages. In addition, both dielectric and magnetic materials in single oxide or complex compound states are all acceptable as long as they are existing on the AC electrodes. This phenomenon has a remarkable significance in fulfilling high-performance supercapacitors and simplifying the electrode improvement in the EDLC fabrication. The high-power energy storage device may be boosted to operate at 3.5 V or higher, 2–3× higher energy density, and >100× longer cycling life with >95% capacitance retention. This investigation is

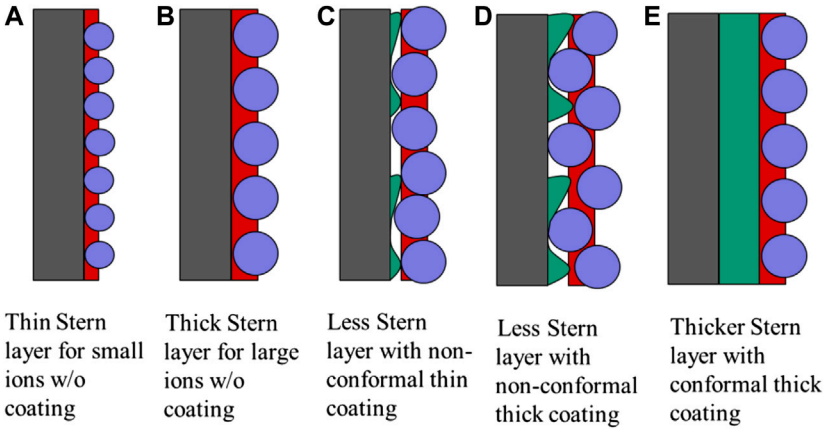

FIGURE 9 | Schematic illustration of the modified Stern layer model.

currently focused on assessing the response of the AC-based supercapacitor device at a voltage stress of 3.5 V. Additional investigation is underway for optimum ALD coating to evaluate the feasibility of the EDLCs at 4 V.

It is well-known that the additional oxide layer deposition is crucial for the electrochemical property improvement of electrodes. A great deal of work has revealed that the ultrathin layer of Al_2O_3 nanoclusters can effectively block the electrolyte's direct contact with the active functional sites thus maintaining cyclic stability and solid electrolyte interphase (SEI) (Sivakkumar et al., 2010). For AC-based supercapacitor, the critical challenge is similar in electrolyte decomposition and the electrochemical polarization on the electrode. The ALD coating renders impressive efficiency in maintaining cycling performance. However, it is still unclear it is due to the suppressed activity of the functional groups by oxide encapsulation or the insertion of an oxide layer that widens the Stern layer thickness.

It was reported that the improved cycling retention of battery cells by Al_2O_3 coating was related to the suppression of oxygen functional groups on activated carbon as revealed by the XPS peak intensities (Zhao and Wang., 2012). However, the electrochemical improvement for Li-ion battery electrodes was found only after 2-cycle coating. The thicker coating after 5-cycle deposition quickly reduces the capacity because of the restricted electron transport and possibly the slower Li ion diffusion kinetics in the thick Al_2O_3 insulating layer. Thereby, thicker oxide coating is not needed despite its additional suppression of the oxygen group. The situation for EDLCs, however, is quite different according to the observed results, where all four types of oxides of 20-cycle ALD deposition (or broad cycle window) on the activated carbons lead to the optimum cycling retention of >95%. The thicker oxide coating becomes necessary for EDLCs regardless of the suppression of the oxygen functional group compared with battery cells. XPS analysis were done for the AC electrode with 20-cycle ALD alumina and those without coating. The O/C ratios before and after ALD modification are 0.3 and 1.65, respectively. The significant increase in oxygen content and bonds indicate the effective ALD modification with aluminum oxide. However, the electrochemical improvement is not sensitive to the dielectric nature of the coating materials. Conductive oxide also results in significantly stable cycling performance at higher voltage. Therefore, a different mechanism is needed to explain the improving effect of thicker coating on the cycling performance of EDLCs.

The authors propose a modification on the Gouy–Chapman-Stern model, where Stern layer thickness and Debye diffuse layer thickness are the basis for the operating voltage window for EDLC (Lyklema., 1995; Zhao and Wang., 2012). The modified Stern layer is corrected as the sum of the additional coating and the original Stern layer defined by the ion radii, as shown in **Figure 9**. Without ALD coating, the Stern layer thickness (d_{Stern}) is entirely determined by the ion nature with or without solvation shell (smaller for aqueous, larger for nonaqueous), as shown in **Figures 9A,B**. For nonaqueous electrolytes, the larger ions are expected to face a thicker Stern layer to withstand a voltage such as 2.7 V or higher. After introducing an additional oxide layer ($d_{coating}$) on the carbon surface, the modified layer (d_{Stern} + $d_{coating}$) is combined by both green and red spacing that is greater against a higher voltage regardless of a conformal coating or not (**Figures 9C–E**). For non-conformal and ultrathin coating as shown in **Figures 9C,D**, the large ions still arrange themselves in a configuration accordingly, thus enabling a relatively larger modified Stern layer thickness to handle higher voltages. With increases in the number of ALD cycles, the oxide layer may exhibit in non-conformal coating (**Figure 9D**) or conformal coating (**Figure 9E**). Any coating thickness may be represented in **Figure 9E**, where a conformal layer separates the electrolyte ions from the AC electrodes. Although a dielectric layer intrinsically withstands a higher voltage before electrical breakdown, it is unnecessary to require a dielectric material with high dielectric strength for EDLC cells because no electron conduction is involved in the case. EDLCs only involves non-faradic charge transfer process, and electron transfer across the electrodes does not occur. This mechanism is different from the Faradaic transfer process occurring in batteries and pseudocapacitors, which involve electron charge accumulation

and electrolyte decomposition. Therefore, the collection of charges is purely electrostatic due to electrolyte ions. The dielectric or conducting oxide layer may act as a spacer between AC and electrolyte to keep the ions farther away from AC. The spacer-thickened Stern layer, along with the Debye diffuse layer, makes cells operate at higher voltages. It is also why better cycling performance is all observed for both the insulating oxide coating and conducting oxide coating.

CONCLUSIONS

This work attempted the ALD coating layer of four different oxide materials to increase the cycling performance at 3.5 V or higher voltages radically. The AC electrodes coated with 2 nm thick oxides effectively maintain the capacitance retention at >95% after 1,000 cycles (>20% higher than uncoated AC electrodes), demonstrating commonalities in the ALD coating effect. Microstructural analyses showed that the ALD coating layer could penetrate the AC electrodes forming a conformal coating on the AC particles. The thin coating was believed to increase the spacing between the AC surface and ions, leading to a modified Stern layer scheme. The proposed modified Stern layer is responsible for the increased cycling performance at operating voltages of >3.5 V and the energy density of 96.2 Wh kg^{-1} is higher than that of commercial EDLC cell by more than eight folds. What matters most for attaining high operating voltage and cycle life appears to be the Stern layer thickness through oxide coatings. However, the insulating materials of thinner coating appear to reduce the electrical impedance more effectively than the conductive coating materials, though all coating materials decrease the leakage current. Therefore, the ALD coating derived better performance may be less associated with the passivation against the surface active sites, different mechanism than that for battery.

DATA AVAILABILITY STATEMENT

The original contributions presented in the study are included in the article/supplementary materials, further inquiries can be directed to the corresponding author/s.

AUTHOR CONTRIBUTIONS

The manuscript was written through the contributions of all authors. All authors have approved the final version of the manuscript.

FUNDING

This research was supported by the 2020 Li Ka Shing Foundation Cross-Disciplinary Research Grant 2020LKSFG01A, and China-Israel Joint Special Research Project Grant 200902154890781.

ACKNOWLEDGMENTS

The authors acknowledge the supply of activated carbon electrodes by Jianghai Capacitor company.

REFERENCES

Arico, C., Ouendi, S., Taberna, P.-L., Roussel, P., Simon, P., and Lethien, C. (2019). Fast electrochemical storage process in sputtered Nb2O5 porous thin films. *ACS Nano.* 13, 5826–5832. doi:10.1021/acsnano.9b01457

Balducci, A., Dugas, R., Taberna, P. L., Simon, P., Plée, D., Mastragostino, M., et al. (2007). High temperature carbon-carbon supercapacitor using ionic liquid as electrolyte. *J. Power Sources.* 165, 922–927. doi:10.1016/j.jpowsour.2006.12.048

Barroso-Bogeat, A., Alexandre-Franco, M., Fernández-González, C., Macías-García, A., and Gómez-Serrano, V. (2014). Electrical conductivity of activated carbon-metal oxide nanocomposites under compression: a comparison study. *Phys. Chem. Chem. Phys.* 16, 25161. doi:10.1039/c4cp03952a

Béguin, F., Presser, V., Balducci, A., and Frackowiak, E. (2014). Supercapacitors: carbons and electrolytes for advanced supercapacitors (Adv. Mater. 14/2014). *Adv. Mater.* 26, 2283. doi:10.1002/adma.201470093

Boukhalfa, S., Evanoff, K., and Yushin, G. (2012). Atomic layer deposition of vanadium oxide on carbon nanotubes for high-power supercapacitor electrodes. *Energy Environ. Sci.* 5, 6872–6879. doi:10.1039/c2ee21110f

Chen, T., Tang, Y.-F., Qiao, Y.-Q., Liu, Z. Y., Guo, W.-F., Song, J.-Z., et al. (2016). All-solid-state high performance asymmetric supercapacitors based on novel MnS nanocrystal and activated carbon materials. *Sci. Rep.* 6, 23289. doi:10.1038/srep23289

Chen, Y., Gao, Z., Zhang, B., Zhao, S., and Qin, Y. (2016). Graphene coated with controllable N-doped carbon layer by molecular layer deposition as electrode materials for supercapacitors. *J. Power Sources.* 315, 254–260. doi:10.1016/j.jpowsour.2016.03.036

Chen, Z., Qin, Y., Amine, K., and Sun, Y.-K. (2010). Role of surface coating on cathode materials for lithium-ion batteries. *J. Mater. Chem.* 20, 7606–7612. doi:10.1039/c0jm00154f

Chi, Y.-W., Hu, C.-C., Shen, H.-H., and Huang, K.-P. (2016). New approach for high-voltage electrical double-layer capacitors using vertical graphene nanowalls with and without nitrogen doping. *Nano Lett.* 16, 5719–5727. doi:10.1021/acs.nanolett.6b02401

Dong, S., He, X., Zhang, H., Xie, X., Yu, M., Yu, C., et al. (2018). Surface modification of biomass-derived hard carbon by grafting porous carbon nanosheets for high-performance supercapacitors. *J. Mater. Chem.* 6, 15954–15960. doi:10.1039/c8ta04080j

Gandla, D., and Tan, D. Q. (2019). Progress report on atomic layer deposition toward hybrid nanocomposite electrodes for next generation supercapacitors. *Adv. Mater. Interfaces.* 6, 1900678. doi:10.1002/admi.201900678

Groner, M. D., Elam, J. W., Fabreguette, F. H., and George, S. M. (2002). Electrical characterization of thin Al_2O_3 films grown by atomic layer deposition on silicon and various metal substrates. *Thin Solid Films.* 413, 186–197. doi:10.1016/S0040-6090(02)00438-8

Hong, K., Cho, M., and Kim, S. O. (2015). Atomic layer deposition encapsulated activated carbon electrodes for high voltage stable supercapacitors. *ACS Appl. Mater. Interfaces.* 7, 1899–1906. doi:10.1021/am507673j

Hulicova-Jurcakova, D., Kodama, M., Shiraishi, S., Hatori, H., Zhu, Z. H., and Lu, G. Q. (2009). Nitrogen-enriched nonporous carbon electrodes with extraordinary supercapacitance. *Adv. Funct. Mater.* 19, 1800–1809. doi:10.1002/adfm.200801100

Ju, Y. F., Wang, M. H., Wang, Y. L., Wang, S. H., and Fu, C. F. (2013). Electrical properties of amorphous titanium oxide thin films for bolometric application. *Adv. Condens. Matter Phys.* 2013, 1–5. doi:10.1155/2013/365475

Jung, Y. S., Lu, P., Cavanagh, A. S., Ban, C., Kim, G.-H., Lee, S.-H., et al. (2013). Unexpected improved performance of ALD coated $LiCoO_2$/graphite Li-ion batteries. *Adv. Energy Mater.* 3, 213. doi:10.1002/aenm.201200370

Kim, M.-H., Yang, J.-H., Kang, Y.-M., Park, S.-M., Han, J. T., Kim, K.-B., et al. (2014). Fluorinated activated carbon with superb kinetics for the supercapacitor application in nonaqueous electrolyte. *Colloid. Surface. Physicochem. Eng. Aspect.* 443, 535–539. doi:10.1016/j.colsurfa.2013.12.020

Kondrat, S., Pérez, C. R., Presser, V., Gogotsi, Y., and Kornyshev, A. A. (2012). Effect of pore size and its dispersity on the energy storage in nanoporous supercapacitors. *Energy Environ. Sci.* 5, 6474–6479. doi:10.1039/c2ee03092f

Kötz, R., and Carlen, M. (2000). Principles and applications of electrochemical capacitors. *Electrochim. Acta.* 45, 2483–2498. doi:10.1016/s0013-4686(00)00354-6

Lanje, A. S., Sharma, S. J., Ningthoujam, R. S., Ahn, J.-S., and Pode, R. B. (2013). Low temperature dielectric studies of zinc oxide (ZnO) nanoparticles prepared by precipitation method. *Adv. Powder Technol.* 24, 331–335. doi:10.1016/j.apt.2012.08.005

Li, Y., Liang, T., Wang, R., He, B., Gong, Y., and Wang, H. (2019). Encapsulation of Fe_3O_4 between copper nanorod and thin TiO_2 film by ALD for lithium-ion capacitors. *ACS Appl. Mater. Interfaces.* 11, 19115–19122. doi:10.1021/acsami.9b03454

Lin, Q., Zhang, J., Kong, D., Cao, T., Zhang, S.-W., Chen, X., et al. (2019). Deactivating defects in graphenes with Al_2O_3 nanoclusters to produce long-life and high-rate sodium-ion batteries. *Adv. Energy Mater.* 9, 1803078. doi:10.1002/aenm.201803078

Liu, C.-F., Liu, Y.-C., Yi, T.-Y., and Hu, C.-C. (2019). Carbon materials for high-voltage supercapacitors. *Carbon.* 145, 529–548. doi:10.1016/j.carbon.2018.12.009

Liu, M., Li, X., Karuturi, S. K., Tok, A. I. Y., and Fan, H. J. (2012). Atomic layer deposition for nanofabrication and interface engineering. *Nanoscale.* 4, 1522–1528. doi:10.1039/c2nr11875k

Lyklema, J. (1995). *Fundamentals of interface and colloid science*. New York, NY: Academic Press, 2, 751.

Ma, S. B., Lee, D. J., Roev, V., Im, D. M., and Doo, S.-G. (2013). Effect of porosity on electrochemical properties of carbon materials as cathode for lithium-oxygen battery. *J. Power Sources.* 244, 494–498. doi:10.1016/j.jpowsour.2013.03.150

Meena, P. L., Screeniva, K., and Kumar, R. (2014). Dielectric properties of spinel Co_3-xMn_xO_4 (x=0.1, 0.4, 0,7, and 1) ceramic compositions. *Indian J. Pure Appl. Phys.* 52, 625–631

Miller, E. E., Hua, Y., and Tezel, F. H. (2018). Materials for energy storage: review of electrode materials and methods of increasing capacitance for supercapacitors. *J. Energy Storage.* 20, 30–40. doi:10.1016/j.est.2018.08.009

Noh, H.-J., Youn, S., Yoon, C. S., and Sun, Y.-K. (2013). Comparison of the structural and electrochemical properties of layered $Li[Ni_xCo_yMn_z]O_2$ (x = 1/3, 0.5, 0.6, 0.7, 0.8 and 0.85) cathode material for lithium-ion batteries. *J. Power Sources.* 233, 121–130. doi:10.1016/j.jpowsour.2013.01.063

Oda, H., Yamashita, A., Minoura, S., Okamoto, M., and Morimoto, T. (2006). Modification of the oxygen-containing functional group on activated carbon fiber in electrodes of an electric double-layer capacitor. *J. Power Sources.* 158, 1510–1516. doi:10.1016/j.jpowsour.2005.10.061

Qian, M., Xu, F., Bi, H., Lin, T., and Huang, F. (2016). Facile sol-gel method combined with chemical vapor deposition for mesoporous few-layer carbon. *Carbon.* 112, 47–52. doi:10.1016/j.carbon.2016.10.093

Safitri, G.-A., Nueangnoraj, K., Sreearunothai, P., and Manyam, J. (2020). Fabrication of activated carbon pouch cell supercapacitor: effects of calendering and selection of separator-solvent combination. *Curr. J. Appl. Sci. Technol.* 20, 124–135. doi:10.14456/cast.2020.2

Shapira, A., Tiurin, O., Solomatin, N., Auinat, M., Meitav, A., and Ein-Eli, Y. (2018). Robust AlF_3 atomic layer deposition protective coating on $LiMn_{1.5}Ni_{0.5}O_4$ particles: an advanced Li-ion battery cathode material powder. *ACS Appl. Energy Mater.* 1, 6809–6823. doi:10.1021/acsaem.8b01048

Shen, H.-H., and Hu, C.-C. (2014). Capacitance enhancement of activated carbon modified in the propylene carbonate electrolyte. *J. Electrochem. Soc.* 161, A1828–A1835. doi:10.1149/2.0681412jes

Simon, P., and Gogotsi, Y. (2020). Perspectives for electrochemical capacitors and related devices. *Nat. Mater.* 19, 1151. doi:10.1038/s41563-020-0747-z

Sivakkumar, S. R., Nerkar, J. Y., and Pandolfo, A. G. (2010). Rate capability of graphite materials as negative electrodes in lithium-ion capacitors. *Electrochim. Acta.* 55, 3330–3335. doi:10.1016/j.electacta.2010.01.059

Smolin, Y. Y., Van Aken, K. L., Boota, M., Soroush, M., Gogotsi, Y., and Lau, K. K. S. (2017). Engineering ultrathin polyaniline in micro/mesoporous carbon supercapacitor electrodes using oxidative chemical vapor deposition. *Adv. Mater. Interfaces.* 4, 1601201. doi:10.1002/admi.201601201

Su, Y., Gu, D., Shao, Y., Wang, X., and Pan, F. (2019). Improved electrochemical performance of $LiNi_{0.5}Mn_{0.3}Co_{0.2}O_2$ electrodes coated by atomic-layer-deposited Ta_2O_5. *Funct. Mater. Lett.* 12, 1850103. doi:10.1142/S1793604718501035

Szymczewska, D., Molin, S., Hendriksen, P., and Jasiński, P. (2017). Microstructure and electrical properties of Fe,Cu substituted $(Co,Mn)_3O_4$ thin films. *Crystals.* 7, 185. doi:10.3390/cryst7070185

Tan, D. Q., and Zhao, R. A. (2014). US Patent 2014/0002956A1.

Vijayan, B. L., Misnon, I. I., Anil Kumar, G. M., Miyajima, K., Reddy, M. V., Zaghib, K., et al. (2019). Facile fabrication of thin metal oxide films on porous carbon for high density charge storage. *J. Colloid Interface Sci.* 562, 567–577. doi:10.1016/j.jcis.2019.11.077

Wang, L., Li, J., He, X., Pu, W., Wan, C., and Jiang, C. (2009). Recent advances in layered LiNi x CoyMn1−x−y O2 cathode materials for lithium ion batteries. *J. Solid State Electrochem.* 13, 1157–1164. doi:10.1007/s10008-008-0671-7

Weingarth, D., Foelske-Schmitz, A., and Kötz, R. (2013). Cycle versus voltage hold - which is the better stability test for electrochemical double layer capacitors?. *J. Power Sources.* 225, 84–88. doi:10.1016/j.jpowsour.2012.10.019

Wu, A.-M., Feng, C.-C., Huang, H., Paredes Camacho, R. A., Gao, S., Lei, M.-K., et al. (2017). Microwave plasma-assisted chemical vapor deposition of porous carbon film as supercapacitive electrodes. *Appl. Surf. Sci.* 409, 261–269. doi:10.1016/j.apsusc.2017.03.017

Xiao, K., Ding, L.-X., Chen, H., Wang, S., Lu, X., and Wang, H. (2015). Nitrogen-doped porous carbon derived from residuary shaddock peel: a promising and sustainable anode for high energy density asymmetric supercapacitors. *J. Mater. Chem.* 4, 372–378. doi:10.1039/C5TA08591H

Yan, J., Fang, Y.-Y., Wang, S.-W., Wu, S.-D., Wang, L.-X., Zhang, Y., et al. (2020). Nitrogen-doped oxygen-rich activated carbon derived from Longan shell for supercapacitors. *Int. J. Electrochem. Sci.* 15, 19821995. doi:10.20964/2020.03.18

Yang, M., and Zhou, Z. (2017). Recent breakthroughs in supercapacitors boosted by nitrogen-rich porous carbon materials. *Adv. Sci.* 4, 1600408. doi:10.1002/advs.201600408

Zhao, J., and Wang, Y. (2013). Surface modifications of Li-ion battery electrodes with various ultrathin amphoteric oxide coatings for enhanced cycleability. *J. Solid State Electrochem.* 17, 1049–1058. doi:10.1007/s10008-012-1962-6

Zhao, J., and Wang, Y. (2012). Ultrathin surface coatings for improved electrochemical performance of lithium ion battery electrodes at elevated temperature. *J. Phys. Chem. C.* 116 (22), 11867–11876. doi:10.1021/jp3010629

Conflict of Interest: The authors declare that the research was conducted in the absence of any commercial or financial relationships that could be construed as a potential conflict of interest.